

ScienceDirect

Procedia CIRP 108 (2022) 665-669



6th CIRP Conference on Surface Integrity

Surface Integrity of Diamond Turned (100)Ge

M. Tunesi^a, D.A. Lucca^{a,*}, M.A. Davies^b, A. Zare^c, M.C. Gordon^a, N.E. Sizemore^b, Y.Q. Wang^d

aSchool of Mechanical and Aerospace Engineering, Oklahoma State University, Stillwater, OK, 74078, USA
bCenter for Precision Metrology, University of North Carolina at Charlotte, Charlotte, NC, 28223, USA
cDepartment of Mechanical Engineering, The Johns Hopkins University, Baltimore, MD, 21218, USA
dDivision of Materials Science and Technology, Los Alamos National Laboratory, Los Alamos, NM, 87545, USA

* Corresponding author. Tel.: +1-405-744-5899. E-mail address: lucca@okstate.edu

Abstract

The resulting surface integrity of (100)Ge subjected to off-axis single point diamond turning was investigated. Feedrate was varied using 9 and 20 μ m/rev at 10 μ m nominal depth of cut. Surface topography was measured with coherence scanning interferometry and atomic force microscopy. The resulting near surface lattice disorder was investigated with channeling Rutherford Backscattering Spectrometry and Raman Spectroscopy. Measured near surface lattice disorder was quantified in terms of equivalent amorphous layer thickness and minimum channeling yield. A comparison of the resulting surface integrity was made with surfaces created by chemomechanical polishing and magnetorheological finishing.

© 2022 The Authors. Published by Elsevier B.V. This is an open access article under the CC BY-NC-ND license (https://creativecommons.org/licenses/by-nc-nd/4.0) Peer review under the responsibility of the scientific committee of the 6th CIRP CSI 2022

Keywords: cutting, surface, surface integrity, germanium, diamond turning

1. Introduction

Freeform optical surfaces are surfaces without an axis of rotational invariance either on or off the surface [1]. To create these surfaces by machining, three axes must be independently used to generate the desired surface [2]. Due to its mechanical and optical properties, single crystal germanium (Ge) is one of the most important infrared (IR) materials used in freeform optics production, with a wide array of applications including thermal imaging devices, night vision systems and IR windows [3]. Although the generation of freeform optics poses a challenge due to their increased geometrical complexity, they allow for precise manipulation of the light path, hence reducing the number of optical elements needed. The introduction of aspheric and freeform optics is disruptive to industry and requires research on more complex manufacturing processes in IR materials to identify and predict cost-effective manufacturing parameters. The only viable method for manufacture of even axisymmetric optics in Ge is

ultraprecision diamond machining. An important aspect towards developing a better understanding of the resulting surfaces created by diamond machining is assessing the resulting surface integrity. A contribution towards such increased understanding is presented here.

In this study single crystal (100)Ge was machined by off-axis cutting with a single crystal diamond round nose tool. Feedrates of 20 μ m/rev and 9 μ m/rev were used. In addition, some of the specimens produced with a feedrate of 9 μ m/rev



Figure 1: Layout of the 8 mm pucks after the initial face turning operation.

were finished by magnetorheological finishing (MRF), chemomechanical polishing (CMP), and CMP followed by chemical etching. The surface topography was characterized by atomic force microscopy (AFM), while the subsurface lattice disorder was characterized by both Raman spectroscopy and channeling Rutherford backscattering spectrometry (RBS).

2. Materials and methods

2.1. Cutting experiments

Single crystal (100)Ge exhibits damage lobes where the surface shows brittle fracture when diamond turned on axis. These damage lobes can be used to identify preferred cutting directions [4]. To confirm these directions, a disk of (100)Ge with a diameter of 7.5 cm was turned on axis by single point diamond turning and the directions were found by evaluating the damage left on the surface. The nominal depth of cut was 0.5 µm and the feedrate was 0.5 µm/rev. The cutting parameters were chosen conservatively to produce a minimally damaged surface. Turning resulted in four primary damage lobes exhibiting the most damage, that were oriented in the <011> cutting direction and four secondary damage lobes with less damage, oriented in the <010> cutting direction. The primary and secondary damage lobes are represented in Fig. 1 by the solid and the dashed lines respectively. A set of specimen pucks, 8 mm in diameter, were then diamond milled with an orientation flat that indicated the cutting direction halfway between <011> and <010>, that would result in the least amount of damage. Cutting experiments were then performed on the pucks by off-axis diamond turning with the cutting direction aligned parallel to the orientation flat. A single crystal diamond tool with a nose radius of 3.0 mm and a rake angle of -25° was used. The nominal depth of cut was 10 μm for all turning experiments. Surfaces were turned using feedrates of 9 μ m/rev and 20 μ m/rev.

2.2. Post processing after cutting

Surfaces that were generated with a feedrate of 9 μ m/rev were further finished with several post polishing processes. The processes included magnetorheological finishing (MRF), chemomechanical polishing (CMP), and CMP followed by chemical etching. The MRF process used a D10 slurry from QED Technologies with an average diamond particle size of

150 nm and a material removal rate of 8 μ m/min. The CMP process used a diluted-bleach and Ultra-Sol S39 (110 nm diameter colloidal silica) slurry with a urethane polishing pad and resulted in a material removal rate of about 6.3 μ m/min. Approximately 18 μ m was removed from the surface during both the CMP and the MRF processes. On one specimen that was polished by CMP, chemical etching was performed with 3% hydrogen peroxide for 2.5 min at room temperature. Based on reported etching rates in the literature, the estimated material removed from the surface was between 50 nm and 75 nm [5]. The specimens investigated are listed in Table 1.

Table 1. Description of the processing parameters used to off-axis turn the (100)Ge specimens.

Specimen	Feedrate [µm/rev]	Post processing	
20 μm as cut	20	None	
9 μm as cut	9	None	
$9 \mu m + MRF$	9	Polished with MRF	
$9 \mu m + CMP$	9	Polished with CMP	
$9 \mu m + CMP + etch$	9	Polished with CMP + etched	

2.3. Surface and subsurface characterization

The surface topography was investigated by both coherence scanning interferometry (CSI) and atomic force microscopy (AFM). The CSI measurements were performed with a 50x objective that resulted in a measurement area of 168 x 168 μm^2 and provided areal surface roughness (Sa) and root mean square areal surface roughness (Sq). For the AFM measurements a commercial Bruker AFM was used in tapping mode to evaluate the Sa and Sq across an area of 40 x 40 μm^2 , as well as for characterizing the overall surface quality.

Subsurface damage was investigated with channeling RBS, performed at Los Alamos National Laboratory. A collimated beam of 2 MeV ⁴He⁺ ions with a spot size of approximately 1 mm² was directed at the specimens, which were aligned with their (100) surface normal to the beam axis and held in a chamber at 4-5×10⁻⁷ Torr. The backscattered particles were collected with a solid-state detector that had a solid angle of 4.2 msr and was positioned 13° off the beam axis. Spectra of the number of backscattered particles vs. backscattered energy were collected to quantify the lattice disorder. The data collected was analyzed using the RUMP code [6]. Confocal Raman spectroscopy was also used to evaluate the lattice

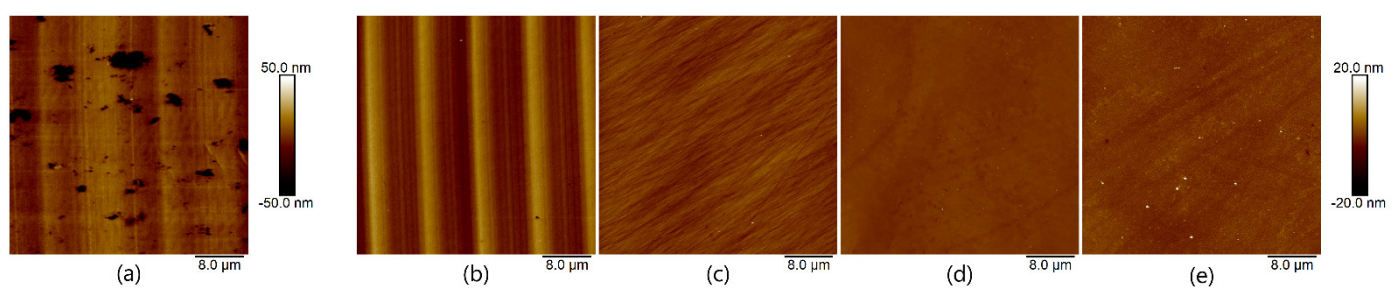


Figure 2: $40 \times 40 \mu m^2$ AFM scans of (100)Ge machined with a feedrate of (a) $20 \mu m$, (b) $9 \mu m$, (c) $9 \mu m$ and then polished by MRF, (d) $9 \mu m$ and then polished by CMP, and (e) $9 \mu m$ and then polished by CMP and etched with H_2O_2 . Note that the 100 nm color scale applies to (a), while the 40 nm scale applies to (b), (c), (d) and (e)

disorder present in the near surface of the machined specimens. A backscattering configuration was used, along with a frequency doubled Nd:YAG laser ($\lambda = 532$ nm) and a Zeiss 100x/0.9NA microscope objective. The 532 nm light has an approximate penetration depth in Ge of 20 nm [7]. A piezoelectrically driven three-axis stage was used to scan the excitation spot over the specimens to obtain area scans. Each scanned area was composed of a grid of individual spectra. To quantify the spatial variations in the Raman response, the microscope software was used to perform Lorentzian curve fittings of the Ge Raman mode for each individual spectrum after the background signal was removed.

3. Results and discussion

3.1. Surface characterization

Figure 2 shows 40 x 40 μm² area scans obtained by AFM where the cutting direction is in the vertical direction of the scan. The surfaces that were not polished resulted in distinguishable and repeatable tool marks with the periodicity of the marks corresponding to the nominal feedrate. The specimen cut with the 20 μm/rev feedrate, shown in Fig. 2(a), resulted in a pitted surface. The pits were uniformly distributed over the surface and varied in size from a diameter of about 1 μm to 5 μm. The average pit depth was 140 nm with respect to the undamaged surface and the maximum depth measured was 445 nm. The surface cut with the 9 µm/rev feedrate, shown in Fig. 2(b), did not show signs of brittle fracture on the surface except for a few pits of a size of less than 1 µm. The surface had well defined peaks and valleys left by the round nose tool shape. The peak to valley height was about 12 nm. Within each cutting mark it was possible to distinguish repeated features that are likely due to small imperfections in the tool. The 9 μm/rev feedrate specimen that was further polished by MRF, shown in Fig. 2(c), did not show any sign of the tool geometry on the surface. The surface showed scratches that were left by the abrasive action of the slurry and were oriented roughly in the same direction. The scratches were uniformly distributed over the surface and most of them were about 1 nm deep with a few having a larger depth of up to 4 nm. The uniformity of the surface resulted in a Sq of 1.2 nm. The 9 µm/rev feedrate specimen further polished by CMP, shown in Fig. 2(d), resulted in a featureless surface and a Sq of 0.5 nm. The 9 $\mu m/rev$ feedrate specimen that was further polished by CMP and then etched, shown in Fig. 2(e), resulted in a slightly higher surface roughness with an Sq of 1.0 nm. Straight scratches with a width of 1 µm were left after the etching process. All three polishing processes removed the tool marks left on the surface by the off-axis cutting, resulting in reduced Sa and Sq values, as summarized in Table 2.

3.2. Subsurface characterization

The resulting subsurface damage was investigated using Raman spectroscopy. Ge typically exhibits a single Raman

mode, the transverse optical mode (TO), centered at $300.7 \pm 0.5 \text{ cm}^{-1}$ [8].

Table 2: Sa and Sq calculated form $40x40~\mu m^2$ AFM scans and $168x168~\mu m^2$ CeV .

Specimen —	AFM		CSI
	Sa [nm]	Sq [nm]	Sq [nm]
20 μm as cut	8.8	24.0	17.3
9 μm as cut	3.1	3.6	3.6
$9 \mu m + MRF$	1.0	1.2	1.0
$9 \mu m + CMP$	0.4	0.5	0.8
9 μm CMP + etch	0.8	1.0	-

This peak has been demonstrated to shift its center to higher wavenumbers due to compressive residual stresses present in the subsurface after machining [9]. The magnitude of the shift can be approximated by a linear relation, $P = 0.26\Delta\omega_{TO}$, where P is in GPa and $\Delta\omega_{TO}$ is in cm⁻¹ [10,11]. The width of the Raman peak can be used qualitatively to evaluate damage in crystals, since it will increase with the amount of disorder [12,13]. To evaluate spatial variations of the Raman peak, area scans were performed on each specimen. The spectra were collected at room temperature, with an integration time of 5 s, and after the objective position was optimized to maximize the 300.7 cm⁻¹ peak intensity. The area scans were created by collecting the Raman spectrum at each point on a grid pattern. The point separation was 0.33 µm. After collection, each spectrum was fit using a Lorentzian function to calculate the peak center and the full width at half maximum (FWHM). The result was then plotted on a color scale map. A 20 x 3 μm² area scan was measured on the specimen cut with a feedrate of 20 μm/rev. The peak center is shown in Fig. 3(a) and the peak

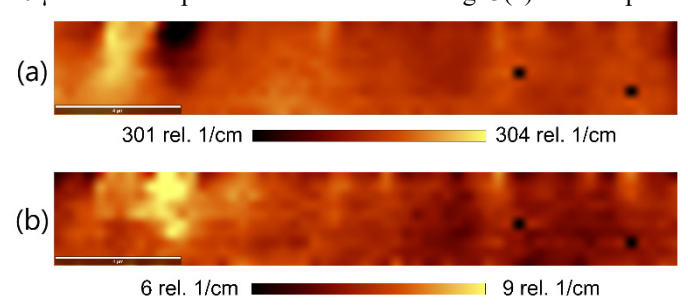


Figure 3: 20 x 3 µm² map of the Lorentzian peak (a) center and (b) FWHM obtained from spectra collected on the specimen cut with a 20 µm/rev feedrate.

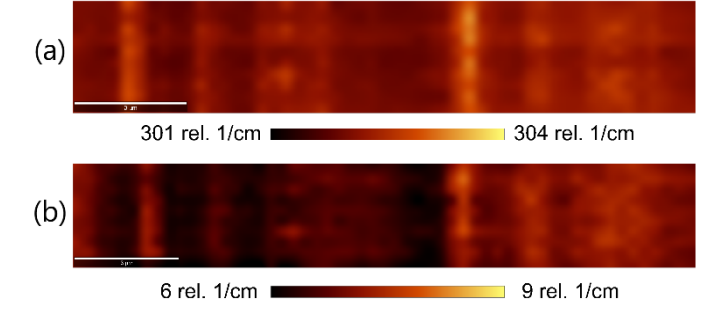


Figure 4: 18 x 3 µm² map of the Lorentzian peak (a) center and (b) FWHM obtained from spectra collected on the specimen cut with a 9 µm/rev feedrate.

width is shown in Fig. 3(b). The scan contains a complete tool mark within its area. When the collection was performed on a grid point far from a pit the peak center was about 302.5 cm⁻¹ and the FWHM was 7.1 cm⁻¹, with small variations depending on the features of the surface. The shift corresponds to 0.47 GPa of compressive stress. In proximity of the pit the peak center shifted to 303.8 cm⁻¹ and the FWHM was 8.2 cm⁻¹, which indicates an increase of the residual stress to 0.81 GPa and an increase of the lattice disorder in the subsurface. Inside the pit the peak center lowered to a minimum of 300.9 cm⁻¹ and the FWHM increased to 10.0 cm⁻¹. This result is consistent with the release of residual stress when brittle fracture occurs, while the damage remains on the surface and in the subsurface. Residual stress was present also in the specimen cut with a 9 μm/rev feedrate, as shown in Fig. 4(a) and 4(b) for peak center and FWHM respectively. The area was 18 x 3 µm² and contained two feed marks. The peak center averaged about 301.8 cm⁻¹ in the valleys, corresponding to 0.29 GPa of residual compressive stress. The peak shifted to 303.2 cm⁻¹ (0.65 GPa) in the high points of the tool marks. The FWHM of the Raman peak also increased from 6.2 cm⁻¹ in the valley to 7.5 cm⁻¹ in the high points, indicating that there was less disorder at the center of the valleys, where the uncut chip thickness is the smallest. Comparing the peak maps confirms that the damage was not only on the surface but propagated below the surface. For the polished specimens, no spatial variation was measured within an 18 x 3 μm² area, confirming that polishing removed the material affected by the cutting operation. The specimen finished by MRF had the Raman peak centered at 300.7 cm⁻¹, corresponding to no residual stress, and a FWHM of 6.0 cm⁻¹. The specimens finished by CMP and CMP + etching had the peak centered at 301.3 cm⁻¹ (0.15 GPa) and 301.0 cm⁻¹ (0.08 GPa) respectively, and both had a FWHM of 5.8 cm⁻¹. This indicates that while there was slight residual stress left in the CMP and CMP + etching specimens, the lattice disorder in the immediate subsurface was smaller when compared to the specimen finished by MRF. The three finishing methods

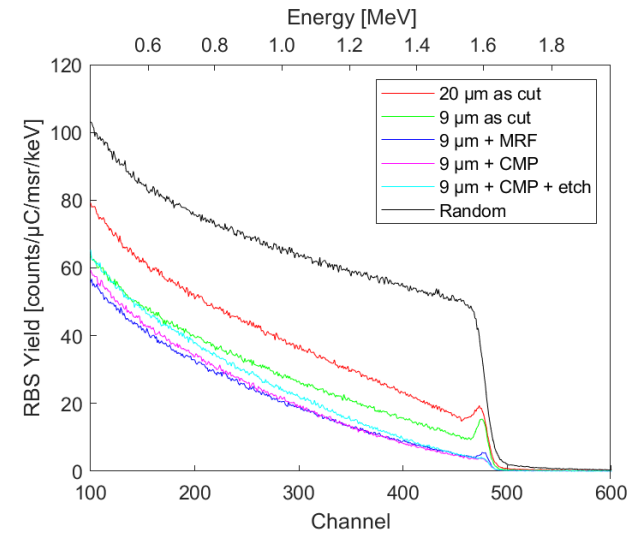


Figure 5: RBS channelling spectra obtained for (100)Ge cut by off-axis turning, with a detector 13° off the beam axis.

produced surfaces with less lattice disorder than the surface after cutting with a feedrate of 9 μ m/rev.

RBS channeling experiments were also performed to quantify the lattice disorder in the machined surfaces. The experiment consisted of aligning a beam of MeV ions with one of the principal planes of symmetry of the Ge lattice (in this case, the normal to the (100) plane). Under channeling conditions some of the ions are backscattered due to collisions with atoms on the surface and in the near surface resulting in a backscattered surface peak. The area under the peak can be related to the amount of lattice disorder. The peak integrated intensity is directly proportional to the number of displaced atoms per cm² [14]. This quantity indicates the number of collisions of the incident beam with the lattice. Another measurement of crystal disorder is χ_{min} [15], which is the ratio of the RBS minimum yield behind the surface peak and the calculated random yield. The theoretical value of a perfect lattice can be computed from first principles using the parameterization tool developed by Doyle [16]. The calculated theoretical minimum yield for a (100)Ge surface is 3.4%. The RBS normalized yield for all the specimens is shown in Fig. 5. Also shown is the random spectrum collected with no crystal alignment (the fundamental RBS spectrum for Ge). The number of backscattered particles (counts) is normalized by the energy per channel (3.113 keV/channel), the detector solid angle (4.2 msr) and the collected charge (12 μ C). The surface peak for the specimen machined with a feedrate of 20 µm/rev exhibited the largest integrated yield, with the surface peak of the specimen machined with a feedrate of 9 µm/rev the next largest. This indicates that the lattice disorder as measured by the number of displaced atoms per cm² increases with feedrate. This is consistent with χ_{min} which is lower for the specimen machined with the lower feedrate. The values obtained for all the specimens are listed in Table 3 including χ_{min} , the surface peak integrated intensity and the conversion of integrated intensity to displaced atoms per cm².

Table 3: Minimum channeling yield (χ_{min}) measured from the normalized RBS yield, and the integrated intensities of the surface peaks.

J				
Specimen	χ _{min} [%]	Integrated area [counts/µC/msr]	Ge atoms/cm ²	
20 μm as cut	31.2	480.4	5.6·10 ¹⁶	
9 μm as cut	19.6	336.9	$4.0 \cdot 10^{16}$	
9 μm MRF	8.8	84.2	$1.0 \cdot 10^{16}$	
9 μm CMP	8.1	33.5	$3.9 \cdot 10^{15}$	
$9 \mu m$ CMP + etch	8.7	24.7	$2.3 \cdot 10^{15}$	
Theoretical (100)Ge [16]	3.4	-	-	

The RBS results agree with the Raman measurements in that the disorder created by off-axis turning was significantly reduced by polishing, as shown by the decrease of both integrated intensity and χ_{min} . The specimen finished by MRF had a larger surface peak, with an integrated intensity of 84.2 counts/ μ C/msr when compared to the CMP and the CMP and etched surfaces, which had 33.5 counts/ μ C/msr and 24.7 counts/ μ C/msr respectively. Since the polishing processes

removed roughly the same amount of material, this indicates that the MRF process resulted in more lattice disorder when compared to the specimens polished by CMP and CMP + etching. The minimum channeling yields for surfaces processed by MRF, CMP and CMP + etching were between 8% and 9%. When compared with the theoretical minimum channeling yield for a perfect (100)Ge surface, this indicates that the surfaces contain a small amount of lattice disorder.

4. Conclusions

Single crystal (100)Ge was diamond turned on axis to identify the most favorable cutting direction. This was found to be halfway between the <010> and <011> directions. The specimens were then diamond milled to create 8 mm diameter, oriented pucks from the diamond turned disk. The pucks were then machined by off-axis diamond turning with feedrates of 20 $\mu m/rev$ and 9 $\mu m/rev$. Surfaces produced with a feedrate of 9 $\mu m/rev$ were also finished by MRF, CMP and a combination of CMP and etching.

AFM measurements showed that the surface produced with a feedrate of 20 $\mu m/rev$ had uniformly distributed fracture, while the one cut with a feedrate of 9 $\mu m/rev$ showed only tool marks with no evidence of brittle fracture. All post processing methods resulted in a flat surface with no sign of the tool path. The specimen finished by MRF had surface scratches while the CMP and CMP + etch specimens did not show any repeated feature on the surface.

Lattice disorder was evaluated using both Raman spectroscopy and channeling RBS. Lattice disorder was larger for the specimen cut with a feedrate of 20 $\mu m/rev$ when compared to the specimen cut with a feedrate of 9 $\mu m/rev$, as indicated by the broadening of the Raman peak in the proximity of fracture and the larger surface peak in the RBS spectrum. The post processed specimens showed very little differences in their respective Raman spectra, but the MRF specimen exhibited a more intense surface peak in the RBS spectrum, which indicated an increased amount of disorder in the near surface.

Acknowledgements

This research was partially supported by the NSF I/UCRC Center for Freeform Optics (IIP-1338877 and IIP-1338898), and NSF grants CMMI-1437225, CMMI-1437232 and CMMI-1727244. This work was performed, in part, at the Center for Integrated Nanotechnologies, an Office of Science User

Facility operated for the U.S. Department of Energy (DOE) Office of Science. Los Alamos National Laboratory, an affirmative action equal opportunity employer, is managed by Triad National Security, LLC for the U.S. Department of Energy's NNSA, under contract 89233218CNA000001.

References

- Fang, F. Z., Zhang, X. D., Weckenmann, A., Zhang, G. X., Evans, C.. Manufacturing and measurement of freeform optics. CIRP Annals, 2013;62/2:823–846.
- [2] Thompson, K. P., Rolland, J. P.. Freeform optical surfaces: a revolution in imaging optical design, Optics and Photonics News, 2012, pp. 30–35.
- [3] Patel, M., Karamalidis, A. K.. Germanium: a review of its US demand, uses, resources, chemistry, and separation technologies. Separation and Purification Technology, 2021;275:118981.
- [4] Nakasuji, T., Kodera, S., Hara, S., Matsunaga, H., Ikawa, N., Shimada, S.. Diamond turning of brittle materials for optical components. CIRP Annals, 1990;39/1:89–92.
- [5] Kagawa, S., Mikawa, T., Kaneda, T.. Chemical etching of germanium with H₃PO₄-H₂O₂-H₂O solution. Japanese Journal of Applied Physics, 1982;21/11R:1616–1618.
- [6] Doolittle, L. R.. Algorithms for the rapid simulation of Rutherford backscattering spectra. Nuclear Instruments and Methods in Physics Research Section B: Beam Interactions with Materials and Atoms, 1985;9/3:344–351.
- [7] Xu, Z., He, Z., Song, Y., Fu, X., Rommel, M., Luo, X., Hartmaier, A., Zhang, J., Fang, F.. Topic review: Application of Raman spectroscopy characterization in micro/nano-machining. Micromachines, 2018;9/7:361.
- [8] Parker, J. H., Feldman, D. W., Ashkin, M., Raman scattering by silicon and germanium. Physical Review, 1967;155/3:712–714.
- [9] Sparks, R. G., Paesler, M. A.. Micro-Raman analysis of stress in machined silicon and germanium. Precision Engineering, 1988:10/4:191–198.
- [10] Olego, D., Cardona, M., Pressure dependence of Raman phonons of Ge and 3C-SiC. Physical Review B - Condensed Matter and Materials Physics, 1982;25/2:1151–1160.
- [11] Asaumi, K., Minomura, S.. Effect of pressure on the Raman shift in Ge. Journal of the Physical Society of Japan, 1978;45/3:1061–1062.
- [12] De Wolf, I., Jian, C., Van Spengen, W. M.. The investigation of microsystems using Raman spectroscopy. Optics and Lasers in Engineering, 2001;36/2:213–223.
- [13] Peercy, P. S.. Raman scattering of ion-implanted GaAs. Applied Physics Letters, 1971;18/12:574–576.
- [14] Lucca, D. A., Wetteland, C. J., Misra, A., Klopfstein, M. J., Nastasi, M., Maggiore, C. J., Tesmer, J. R.. Assessment of subsurface damage in polished II-VI semiconductors by ion channeling. Nuclear Instruments and Methods in Physics Research Section B: Beam Interactions with Materials and Atoms, 2004;219–220:611–617.
- [15] Leo, G., Drigo, A. V., Lovergine, N., Mancini, A. M.. Structural characterization of CdS epilayers by channeling Rutherford backscattering spectrometry. Journal of Applied Physics, 1998;70/4:2041–2045.
- [16] Doyle, B. L.. Parameterization of ion channeling half-angles and minimum yields. Nuclear Instruments and Methods in Physics Research Section B: Beam Interactions with Materials and Atoms, 2016;371:63– 68.